

# Pumping dynamics of nuclear spins in GaAs quantum wells

Raphael W. Mocek,<sup>\*</sup> Danil O. Tolmachev, Giovanni Cascio, and Dieter Suter<sup>†</sup>  
*Experimental Physics III, TU Dortmund University, Otto-Hahn-Str. 4a, 44227 Dortmund, Germany*  
 (ΩDated: August 3, 2018)

Irradiating a semiconductor with circularly polarized light creates spin-polarized charge carriers. If the material contains atoms with non-zero nuclear spin, they interact with the electron spins via the hyperfine coupling. Here, we consider GaAs/AlGaAs quantum wells, where the conduction-band electron spins interact with three different types of nuclear spins. The hyperfine interaction drives a transfer of spin polarization to the nuclear spins, which therefore acquire a polarization that is comparable to that of the electron spins. In this paper, we analyze the dynamics of the optical pumping process in the presence of an external magnetic field while irradiating a single quantum well with a circularly polarized laser. We measure the time dependence of the photoluminescence polarization to monitor the buildup of the nuclear spin polarization and thus the average hyperfine interaction acting on the electron spins. We present a simple model that adequately describes the dynamics of this process and is in good agreement with the experimental data.

PACS numbers: 78.67.De, 78.55.Cr, 78.66.Fd, 76.60.-k

Keywords: Optical Orientation, Semiconductors, Optical Pumping, Spin Dynamics

## I. INTRODUCTION

Optical pumping creates electrons and holes in semiconductor samples with spin polarizations far from equilibrium, as shown by the level scheme and transition diagram of fig. 1. Depending on the conduction- and valence-band states involved in the optical transition, the polarization of the electron spins can reach almost 100% [1].

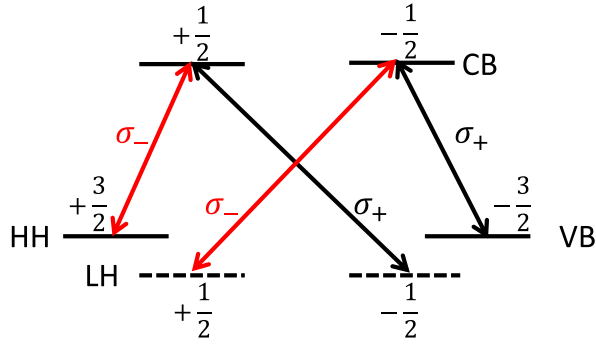


FIG. 1. Selection rules for the optical transitions between the valence-band (VB) and the conduction-band (CB) of a semiconductor quantum well. The confinement lifts the degeneracy of the hole states. (modified after [2])

The spin-polarization of the conduction-band electrons can be monitored through the photoluminescence (PL) polarization [3–5]

$$DOP = \frac{I(\sigma_+) - I(\sigma_-)}{I(\sigma_+) + I(\sigma_-)}, \quad (1)$$

where  $I(\sigma_{\pm})$  is the intensity of right- or left-circularly polarized PL.

In many materials, and in particular in the GaAs quantum wells that we consider in this work, the electrons are coupled to different nuclear spins by the hyperfine interaction. Accordingly, the electron spin orientation can be transferred to the nuclear spins [6–9] in a process known as dynamic nuclear polarization (DNP) [2, 10, 11]. Conversely, the ensemble of polarized nuclear spins affect the evolution of the electron spins. The overall effect can be summarized by an effective nuclear magnetic field [10, 12–17]. This is used, e.g., in optically detected nuclear magnetic resonance [6, 13, 18–22].

The goal of this study is a detailed understanding of the buildup of the nuclear spin polarization during optical pumping. For this purpose, we rely mostly on measurements of the time dependence of the PL polarization, from which we determine the buildup of the nuclear magnetic field. The paper is organized as follows. In Sec. II, we describe a simple model of the spin dynamics during optical pumping. In Sec. III we present the experimental setup and the sample under investigation. Section IV A contains the experimental results for the time dependence of the optical pumping process and compares them to the theoretical prediction. Section IV B summarizes the effect of the control parameters laser intensity and optical detuning on the optical pumping dynamics. The paper ends with a short discussion and conclusions.

## II. THEORY

### A. Electron spin polarization

The optical pumping process, as well as the optical detection couple the photon angular momentum directly to the spin of the charge carriers. We therefore start with the equation of motion for the spin density operator  $\rho$ :

<sup>\*</sup> raphael.mocek@tu-dortmund.de

<sup>†</sup> dieter.suter@tu-dortmund.de

$$\frac{\partial \rho}{\partial t} = -\frac{i}{\hbar} [\mathcal{H}, \rho] - \Gamma_R \rho - \Gamma_S \left( \rho - \frac{\text{Tr}\{\rho\}}{2} \mathbb{1} \right) + \tilde{P} \quad (2)$$

$$\mathcal{H} = \hbar \gamma_e \vec{B} \cdot \vec{S}$$

We use the spin operators defined as  $S_i = \frac{1}{2} \sigma_i$  with  $i \in [x, y, z]$ ,  $\gamma_e$  is the gyromagnetic ratio of the conduction electrons and  $\mathbb{1}$  is the two-dimensional unity matrix.  $\vec{B}$  is the magnetic field,  $\Gamma_R$  describes the recombination of the electrons from the conduction- to the valence-band and  $\Gamma_S$  the spin relaxation rate. The matrix  $\tilde{P}$  describes the buildup of electron spin density by the absorption of circularly polarized photons. In the coordinate system defined in fig. 2, this matrix is

$$\tilde{P} = P \begin{pmatrix} \cos^2 \frac{\Theta_L}{2} & \frac{1}{2} \sin \Theta_L \\ \frac{1}{2} \sin \Theta_L & \sin^2 \frac{\Theta_L}{2} \end{pmatrix}. \quad (3)$$

$P$  is the rate at which the optical pumping process generates electron spin density in the conduction band.  $\Theta_L$  is the angle between the incident laser beam and the z-axis, as defined in fig. 2.

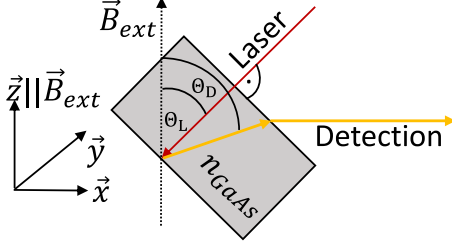


FIG. 2. Schematic overview of the chosen coordinate system and the relevant angles. The laser light hits the sample perpendicularly.

If the nuclear spins are polarized, they collectively modify the effective magnetic field acting on the electron spin. We therefore write the total field  $\vec{B}$  as the sum of the external field  $\vec{B}_{ext}$  and the nuclear field  $\vec{B}_{nuc}$ . In our coordinate system, both are oriented along the z-axis and we therefore write  $B_{ext} + B_{nuc}$  for the z-component of the effective magnetic field. Under stationary conditions, the expectation values of the three components of the electron spin are

$$\begin{aligned} \langle S_x \rangle &= \text{Tr}\{S_x \rho\} = \frac{P}{2\gamma_e} \frac{\Delta B \sin \Theta_L}{(B_{ext} + B_{nuc})^2 + \Delta B^2} \quad (4) \\ \langle S_y \rangle &= \text{Tr}\{S_y \rho\} = \frac{P}{2\gamma_e} \frac{(B_{ext} + B_{nuc}) \sin \Theta_L}{(B_{ext} + B_{nuc})^2 + \Delta B^2} \\ \langle S_z \rangle &= \text{Tr}\{S_z \rho\} = \frac{P}{2\gamma_e} \frac{\cos \Theta_L}{\Delta B}. \end{aligned}$$

Here the parameter  $\Delta B$  is defined as  $\Delta B = \frac{\hbar(\Gamma_R + \Gamma_S)}{|g^*| \mu_B}$  with  $g^*$  as the g-factor of the conduction electrons [23–25]

and  $\text{Tr}\{\rho\} = \frac{P}{\Gamma_R}$ . In our case, the direction of detection  $\vec{e}$  is close to the x-axis

$$\vec{e} = (\sin \Theta_D, 0, \cos \Theta_D), \quad (5)$$

where the angle  $\theta_D$  is defined in fig. 2.

Experimentally, we measure the degree of photon polarization (see eq. (1)) in the direction  $\vec{e}$  by dividing the difference between the two intensities  $I(\sigma_{\pm})$  by their sum. The result is

$$\begin{aligned} S_D &= \frac{1}{\text{Tr}\{\rho\}} (\sin \Theta_D \langle S_x \rangle + \cos \Theta_D \langle S_z \rangle) \\ &= S_0 \left( \cos \Theta_L \cos \Theta_D + \frac{\Delta B^2 \sin \Theta_L \sin \Theta_D}{\Delta B^2 + (B_{ext} + B_{nuc})^2} \right) \quad (6) \end{aligned}$$

Here  $S_0 = \frac{1}{2} \frac{\Gamma_R}{\Gamma_R + \Gamma_S}$  describes the equilibrium spin polarization in the absence of a magnetic field. This signal, measured as a function of the external magnetic field, is known as a (shifted) Hanle curve. It represents a Lorentzian, with a maximum at  $B_{ext} = -B_{nuc}$  and a width  $\Delta B$ .

## B. Nuclear spin polarization

In this study, we concentrate on the evolution of the nuclear spin polarization. The equation of motion for the nuclear spin populations can be written as

$$\frac{d}{dt} \begin{pmatrix} p_{\uparrow} \\ p_{\downarrow} \end{pmatrix} = \begin{pmatrix} -\kappa s_{\downarrow} - \frac{1}{2T_1} & \kappa s_{\uparrow} + \frac{1}{2T_1} \\ \kappa s_{\downarrow} + \frac{1}{2T_1} & -\kappa s_{\uparrow} - \frac{1}{2T_1} \end{pmatrix} \begin{pmatrix} p_{\uparrow} \\ p_{\downarrow} \end{pmatrix}, \quad (7)$$

where  $\kappa$  is the transfer rate at which electronic and nuclear spins undergo mutual flip-flop transitions and  $s_{\uparrow\downarrow}$  are the densities of the electron spins generated by the optical pumping process. According to eq. (4) they are

$$s_{\uparrow\downarrow} = \frac{P}{2\Gamma_R} \pm \langle S_z \rangle.$$

For quantum wells with dimensions of  $\approx 20$  nm, the recombination rate of the electrons is  $\Gamma_R \approx 10^9 \text{ s}^{-1}$  [26]. For time-independent parameters, eq. (7) can be solved analytically. If the system is initially in thermal equilibrium,  $p_{\uparrow\downarrow}(0) = 0.5$ , the solution is

$$p_{\uparrow\downarrow}(t) = \frac{1 \pm \Delta p(t)}{2}, \quad (8)$$

where the population difference is

$$\Delta p(t) = \Delta p_{\infty} \left( 1 - e^{-\left(\frac{1}{T_1} + \kappa \frac{P}{\Gamma_R}\right)t} \right) \quad (9)$$

and its equilibrium value

$$\Delta p_{\infty} = \langle S_z \rangle \frac{2\kappa T_1 \Gamma_R}{\Gamma_R + \kappa T_1 P}. \quad (10)$$

The nuclear spin polarization can be measured through its effect on the electron spin, via the effective nuclear field

$$\begin{aligned} B_{nuc}(t) &= B_{max}\Delta p(t) \\ &= B_{max}\Delta p_{\infty} \left(1 - e^{-\left(\frac{1}{T_1} + \kappa\frac{P}{\Gamma_R}\right)t}\right). \end{aligned} \quad (11)$$

According to eq. (6),  $B_{nuc}$  is given by the maximum of the Hanle curve. To measure the time dependence of the populations of the nuclear spin, we therefore measure the Hanle curves for different pumping times.

### III. EXPERIMENTAL

The sample used for this investigation was grown by molecular beam epitaxy on a Te-doped GaAs substrate. It consists of 13 undoped GaAs/Al<sub>0.35</sub>Ga<sub>0.65</sub>As quantum wells with thicknesses  $d$  ranging from 2.8 to 39.3 nm [27].

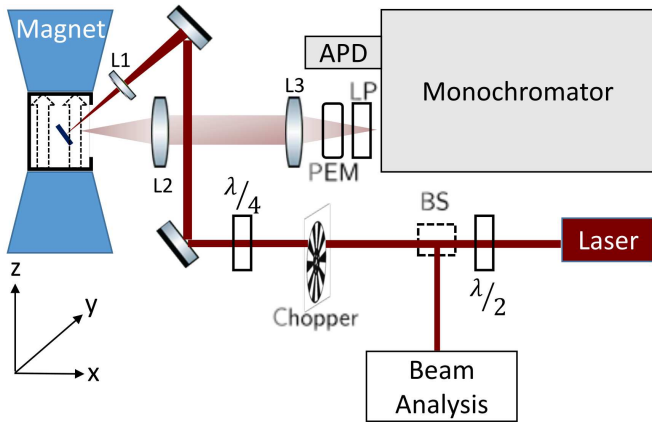


FIG. 3. Experimental setup of the optical pumping experiment. L1, L2 and L3: lenses, LP: linear polarizer, PEM: photo elastic modulator, APD: avalanche photo diode, BS: beam splitter,  $\lambda/2$ ,  $\lambda/4$ : retardation plates.

Figure 3 shows a schematic representation of the experimental setup. For the optical excitation we use a semiconductor laser (Toptica DLC DL PRO), which covers the wavelength range of  $\lambda_{exc} = 799 - 812$  nm. The magnetic field is created by a resistive electromagnet (Bruker) with a range of  $B_{ext} = 0$  T – 1.4 T. The sample is mounted on the cold finger of a home-built flow-cryostat and kept at temperatures of  $T \approx 4.7 \pm 0.3$  K. The laser beam analysis includes a spectrometer (APE waveScan USB) for monitoring the laser wavelength and a photodiode to monitor the laser power. The PL is passed through a monochromator (Spex 1704) and a photoelastic modulator (Hinds Instruments PEM 90) and detected with an avalanche photodiode (APD, Hamamatsu 5640). Two lock-in amplifiers (Stanford Research SR830 DSP) are then used to measure the total PL power

$I_{\Sigma} = I(\sigma_{+}) + I(\sigma_{-})$  and the difference between right- and left-circularly polarized light  $I_{\Delta} = I(\sigma_{+}) - I(\sigma_{-})$ .

The optical pumping process took place in constant external magnetic fields of  $B_{ext} = 0.3$  T or 1 T. We monitored the buildup of the nuclear spin polarization by measuring Hanle curves [2, 28] as a function of the pumping time. For the Hanle curves, the magnetic field was scanned from  $B_{ext}$  either upward or downward, depending on the displacement of the Hanle curve. The time for measuring a Hanle curve was about 10 s, short compared to the duration of the optical pumping. During the Hanle measurements, the laser power was reduced to  $P_L \approx 2$  mW, to minimize the optical pumping effects. The angles defined in fig. 2 were  $\Theta_D = 81^\circ$  and  $\Theta_L = 78^\circ$  for all experiments.

### IV. RESULTS

#### A. Nuclear field buildup

The main goal of these experiments was a quantitative understanding of the process that generates the nuclear spin polarization. For this purpose, we performed a set of measurements that consisted of a pumping period  $T_{pump}$  during which the sample was irradiated with circularly polarized light in a constant magnetic field. Immediately after this pumping period, we performed a rapid scan of the magnetic field to measure a Hanle curve. According to eq. (4), the maxima of these curves correspond to the effective nuclear field  $|B_{nuc}|$  and can therefore be used as a probe of the nuclear spin polarization. Measured Hanle curves after two different times  $T_{pump}$  are shown in fig. 4 (a). The experimental parameters for these measurements are  $B_{ext} = 1$  T and laser power  $P_L = 49$  mW. The monochromator was set to the maximum of the PL line of the  $d = 19.7$  nm quantum well and the optical detuning of the laser beam was  $\Delta\lambda = \lambda_{det} - \lambda_{exc} = 811.6$  nm – 811.3 nm = 0.3 nm.

Figure 4(b) shows the buildup of the effective nuclear field  $|B_{nuc}(t)|$ . It compares the experimental data with the theoretical curve calculated from eq. (11). For the parameters, we used a spin-lattice relaxation time of  $T_1 = 596 \pm 160$  s, which we measured independently, and is comparable to literature values for similar systems [29]. From the fitted curve and our experimental parameters, we calculated  $P = 7.7 \cdot 10^{13} \frac{\#e^-}{s \cdot \mu m^3}$ . Table I shows the other relevant parameters determined from these curves.

$B_{max}$ [T]	$\Delta p_{\infty}$ [%]	$\kappa \left[ \frac{\mu m^3}{s \cdot \#e^-} \right]$
29	3.4	$6.8 \cdot 10^{-8}$

TABLE I. Fit parameters for the data shown in fig. 4(b).

The fit-result for the maximum field  $B_{max}$  is significantly larger than some values from the literature [2, 12]. The buildup of the nuclear spin polarization can also be

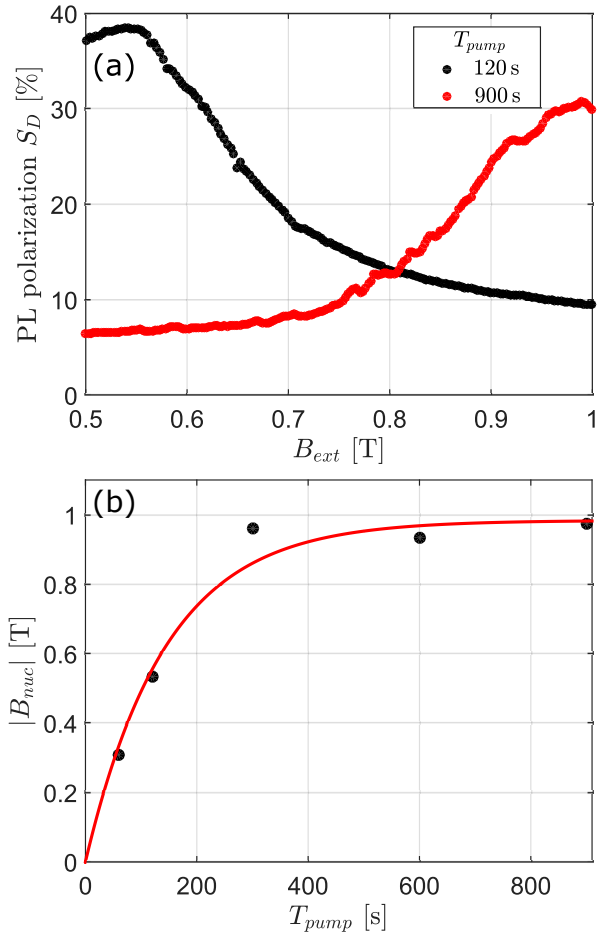


FIG. 4. Time dependence of the effective nuclear field  $|B_{nuc}|$ : (a) Hanle curves measured after optical pumping periods of  $T_{pump} = 120$  s and 900 s. (b) Evolution of the nuclear field during the optical pumping. The solid red line is the fit result using eq. (11) and the filled circles represent the experimental values.

monitored through the time dependence of the PL polarization during the optical pumping process, as shown in fig. 5. The theoretical curve was calculated from eqs. (6) and (11) with the parameters of tab. I.

### B. Dependence on the laser intensity

The parameter  $P$  introduced in eq. (3) describes the rate at which electron spin density is created in the material. Over some range, we therefore expect that  $P$  should be proportional to the laser power  $P_L$ . Since only absorbed photons generate electron spins, the rate should also depend on the absorption probability of the photons and reach a maximum at the optical resonance. The influence of optical detuning is discussed in Sec. IV C.

We examined the dependence of the pumping dynamics on the laser power by performing a series of measurements with increasing laser intensity. After

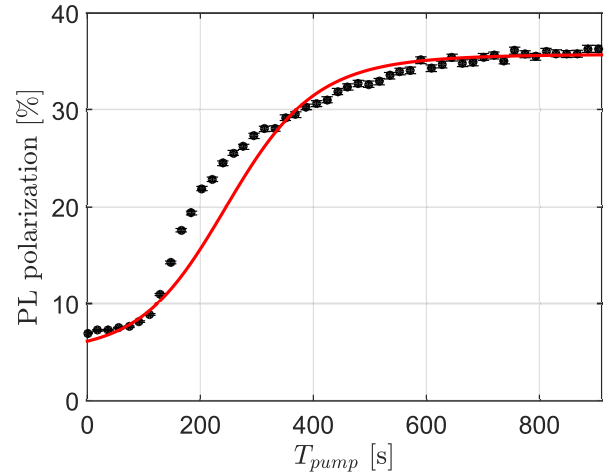


FIG. 5. Time dependence of the optical pumping process: measured PL polarization under optical pumping conditions with  $B_{ext} = 1$  T,  $P_L = 49$  mW and  $\Delta\lambda = 0.3$  nm. The solid red line was calculated with the parameters of table I using eq. (6) and (11).

pumping times  $T_{pump} = [30$  s, 60 s, 180 s, 300 s, 600 s], we measured Hanle curves to monitor the evolution of the effective nuclear magnetic field  $|B_{nuc}|$ . We repeated this procedure with laser powers of  $P_L = [20$  mW, 25 mW, 30 mW, 35 mW, 40 mW]. Further experimental parameters were  $B_{ext} = 0.3$  T and  $\Delta\lambda = 0.5$  nm. The detection wavelength was  $\lambda_{det} = 811.6$  nm, which corresponds to the maximum of the PL line of the  $d = 19.7$  nm quantum well.

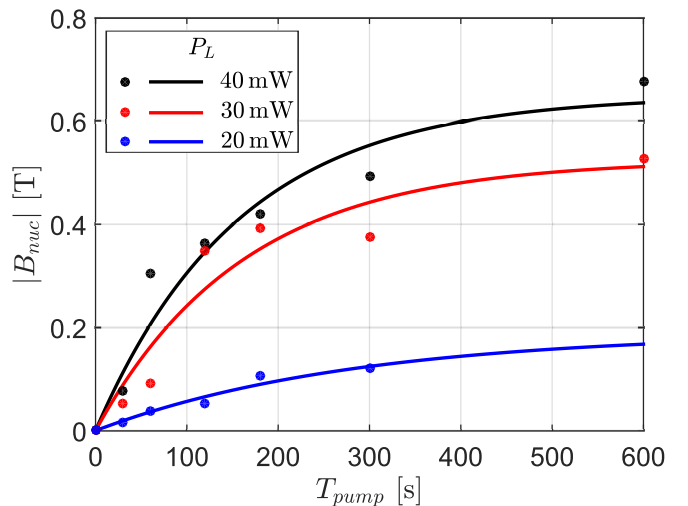


FIG. 6. Evolution of the effective nuclear magnetic field  $|B_{nuc}|$  for different laser powers  $P_L$ . The circles mark the experimental data while the solid lines are the result of the fit using eq. (11) and  $B_{max} = 5.3$  T,  $\kappa = 6.3 \cdot 10^{-8} \frac{\mu\text{m}^3}{\text{s}\cdot\#e^-}$  as fixed parameters.

Figure 6 shows the buildup of the effective nuclear mag-

netic field  $|B_{nuc}(t)|$  for different laser intensities. The experimental data, which are shown as circles, are the maxima of the Hanle curves taken after each optical pumping period  $T_{pump}$ . We used  $B_{max} = 29$  T and  $\kappa = 6.8 \cdot 10^{-8} \frac{\mu\text{m}^3}{\text{s} \cdot \#e^-}$  as fixed parameters obtained by the measurement presented in Sec. IV A and eq. (11) to fit the experimental data shown in fig. 6. The resulting  $|B_{nuc}(t)|$  are shown as solid curves.

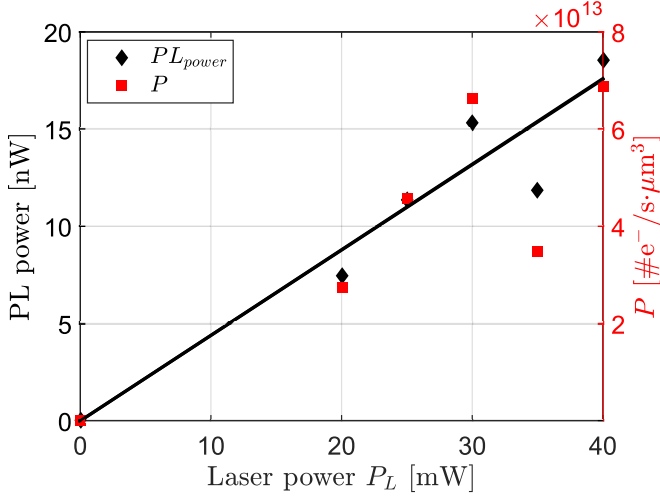


FIG. 7. Rate of change in electron spin density  $P$  together with the PL light power as a function of the laser power  $P_L$ . The solid line is the result of the linear fit.

From the observed buildup-rate of  $|B_{nuc}|$ , we calculated the rate  $P$  at which electron-spin density is generated by the pumping process. Figure 7 shows the resulting rates  $P$  as a function of the laser power  $P_L$ . The rate at which electrons are generated in the conduction-band should also be reflected in the PL power, which we measured independently. As shown in fig. 7, both quantities are roughly proportional to the laser power, with proportionality factors  $m_P = (1.7 \pm 0.5) \cdot 10^{12} \frac{\#e^-}{\text{s} \cdot \mu\text{m}^3 \cdot \text{mW}}$  and  $m_{PL_{power}} = 0.4 \pm 0.1 \frac{\text{nW}}{\text{mW}}$ , respectively.

### C. Optical detuning

The rate  $P$  at which electron-spins are generated depends also on the frequency of the laser with respect to the resonance frequency of the quantum well. We measured the time dependence of the PL polarization under optical pumping conditions for different optical detunings  $\Delta\lambda = [0.7 \dots 2.1]$  nm relative to the peak wavelength  $\lambda_{det} = 811.6$  nm of the  $d = 19.7$  nm quantum well. The experimental parameters were  $B_{ext} = 0.3$  T and  $P_L = 47$  mW.

Figure 8 shows some of the measured curves. The experimental data are compared to the theoretical expectations calculated from eq. (6) and (11), using the experimental parameters of our system and the fit parameters

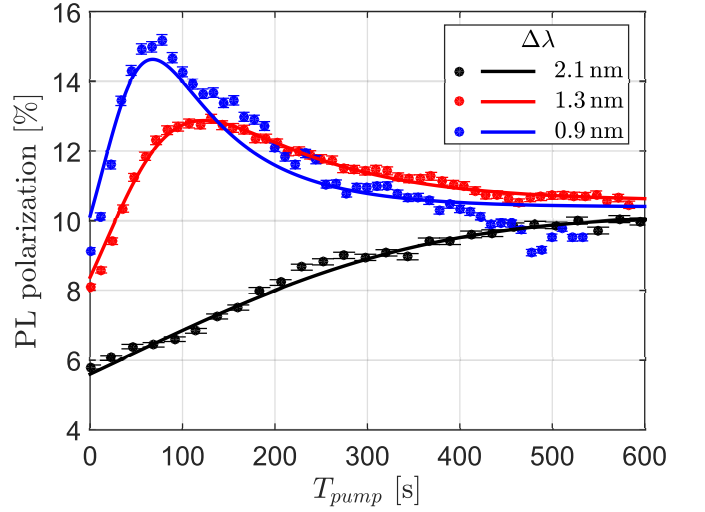


FIG. 8. Time dependence of the optical pumping process: measured PL polarization under optical pumping conditions with  $B_{ext} = 0.3$  T,  $P_L = 47$  mW and  $T_{pump} = 600$  s for different optical detunings  $\Delta\lambda$ . The solid lines are the fit results based on eq. (11),(6).

given in tab. I. The electron-spin density generation rate  $P$  was adjusted for the curves to fit the experimental data.

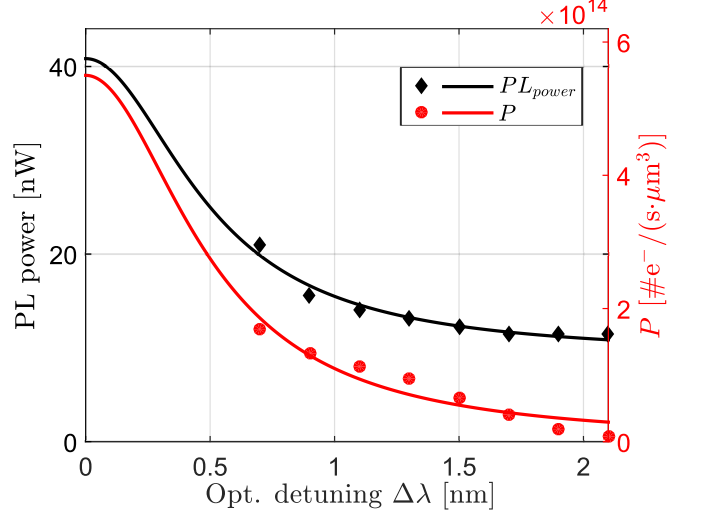


FIG. 9. Detuning dependence of the rate of change in electron spin density  $P$ : the circles mark the fit-parameters  $P$  and the solid red line is the result of the Lorentzian fit function eq. (12). Detuning dependence of the PL light power: the diamonds mark the measured PL light power and the solid black line is given by eq. (13).

Figure 9 shows the resulting fit-parameters  $P$  as red circles for the complete set of measurements as a function of the laser detuning  $\Delta\lambda$ . We compare the experimental

data points to a Lorentzian,

$$P(\Delta\lambda) = \frac{a_1}{\left(\frac{\Delta\lambda}{HWHM}\right)^2 + 1}. \quad (12)$$

Fitting the data marked as circles in fig. 9 to eq. (12) results in  $a_1 = (5.5 \pm 0.9) \cdot 10^{15} \frac{\#e^-}{s \cdot \mu\text{m}^3 \cdot \text{nm}}$  and a half width at half maximum  $HWHM = (0.5 \pm 0.1) \text{ nm}$ .

The number of photons absorbed by the QW should also be reflected in the rate of emitted PL. We therefore also measured the average PL power as a function of the detuning  $\Delta\lambda$ . The results are shown in fig. 9 as black diamonds. We compare them to the theoretically expected behavior of a Lorentzian line similar to eq. (12), but with an additional offset  $PL_{off}$  reflecting the effect of non-resonant excitation:

$$PL_{power}(\Delta\lambda) = \frac{a_2}{\left(\frac{\Delta\lambda}{0.5 \text{ nm}}\right)^2 + 1} + PL_{off}. \quad (13)$$

The fit result is shown in fig. 9 as a solid black line using the fit-parameters  $PL_{power}(\Delta\lambda = 0) \approx 40.8 \text{ nW}$ ,  $a_2 = 31.7 \pm 2.1 \text{ nW}$  and  $PL_{off} = 9.2 \pm 0.8 \text{ nW}$ . The value of  $PL_{off}$  was also measured independently by exciting the system with a blue laser with  $\lambda_{exc} = 406 \text{ nm}$  and a laser power of  $P_L = 10 \text{ mW}$ . We obtained a PL power that was compatible with the value given above and found no significant PL polarization, which is consistent with the above assumption that the non-resonant processes should not contribute to the spin density [21].

#### D. Influence of the laser beam cross section

Figure 10 shows a representative series of Hanle curves measured for different pumping times  $T_{pump}$  in an external field  $B_{ext} = 0.3 \text{ T}$  with a laser power of  $P_L = 39 \text{ mW}$ . Similar to the data shown above, they show a buildup of nuclear spin polarization, manifested as a shift of the maximum towards higher fields. Compared to the data shown above, the monochromator was set to the PL maximum of the  $d = 39.1 \text{ nm}$  quantum well, and the optical detuning of the laser was  $\Delta\lambda = 7 \text{ nm}$ , which resulted in correspondingly lower PL polarization. We used smaller increments for  $T_{pump}$  in order to achieve higher temporal resolution of the pumping process. Using eq. (6), we fitted each curve separately to the theoretical shape, adding an offset of 0.3 %, which may be due to stray light. As shown in fig. (10), we find the expected increase of the nuclear field with the pumping time. In addition, the curves broaden and the maximum of the polarization decreases with increasing pumping time. To understand these additional effects, we consider the intensity distribution over the laser beam cross section, which we assume to be Gaussian. As a result of this distribution, different sample regions experience different intensities resulting in different pumping rates. To describe this effect, we write the laser intensity as a function of the

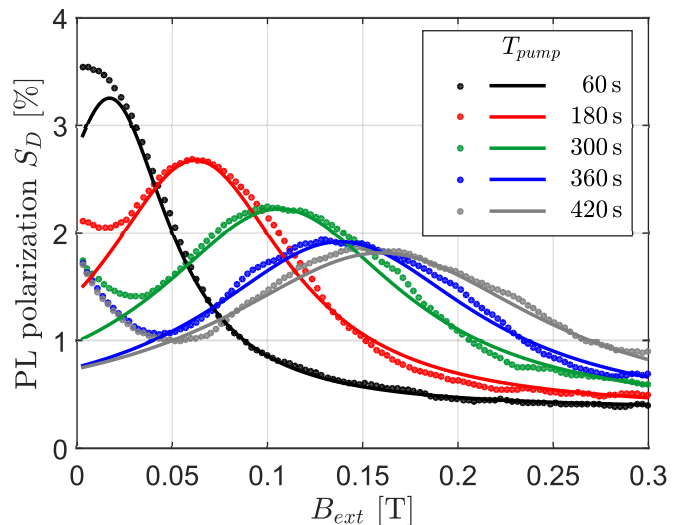


FIG. 10. Shifted Hanle curves: measured data and calculated Hanle curves based on the fit-parameters shown in fig. 12.

distance  $r$  from the center of the beam as

$$I(r) = I_0 \cdot e^{-\frac{r}{2\sigma_0^2}}, \quad (14)$$

with the maximum intensity

$$I_0 = \frac{P_L}{2\pi\sigma_0^2}. \quad (15)$$

For a laser power  $P_L = 39 \text{ mW}$  and beam width  $\sigma_0 = 88 \mu\text{m}$ , we obtain  $I_0 = 0.8 \frac{\mu\text{W}}{\mu\text{m}^2}$ . For a numerical simulation of the observed Hanle curves, we calculated the pumping dynamics and resulting Hanle curves  $h(B_{ext}, I(r))$  for annular segments of the laser beam using eq. (6). The individual curves were then weighted with the PL power  $I(r) r dr$  emitted by each ring. The resulting calculated Hanle curve is

$$S_C = \frac{\int dr h(B_{ext}, I(r)) r I(r)}{\int dr r I(r)}. \quad (16)$$

Figure 11 shows the calculated Hanle curves  $S_C$  for increasing times  $T_{pump} = [0 \dots 2000] \text{ s}$ . The saturation of the nuclear field  $B_{nuc}$  as well as the broadening of the curves and the decrease in the maximal degree of PL polarization are clearly visible. Figure 12 compares the predictions from this simple model with the experimental Hanle curves. The decreasing maximal degree of PL polarization and the broadening of the curves, represented by  $\Delta B$ , as well as the shift of the maxima,  $|B_{nuc}|$ , are qualitatively well described by the theoretical model. Figure 13 summarizes this model in a different way: it shows the variation of the effective field  $B_{ext} + B_{nuc}$  over the laser beam cross section. The dependence of the effective field on the position  $r$  is calculated for two different pumping times,  $T_{pump} = 36 \text{ s}$  (solid red line) and  $T_{pump} = 271 \text{ s}$  (dashed red line) with an external field of  $B_{ext} = 0.5 \text{ T}$ , and a laser power of  $P_L = 49 \text{ mW}$ .

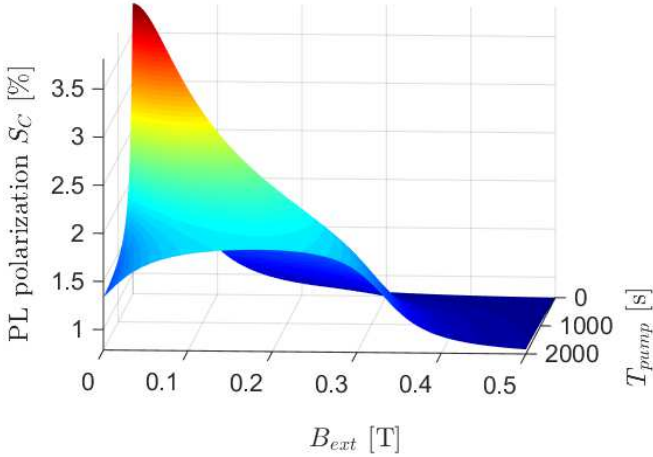


FIG. 11. Calculated Hanle curves  $S_C$  for increasing times  $T_{pump} = [0...2000]$  s.

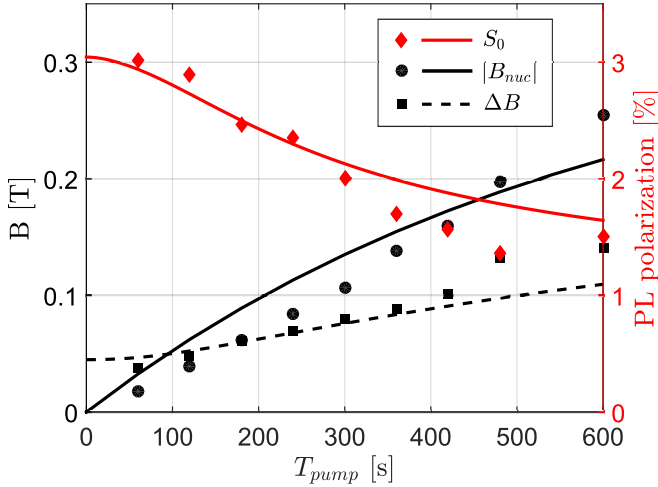


FIG. 12. Comparison between the experimental parameters  $|B_{nuc}|$ ,  $\Delta B$  and  $S_0$  obtained by fitting the Hanle curves shown in fig. 10 (a) using eq. (6) with the result of the simulation.

## V. DISCUSSION AND CONCLUSION

As we have shown, our experimental setup allows one to measure the optical pumping dynamics of nuclear spins in GaAs quantum wells. We presented a simple theoretical model that describes the buildup of the nuclear spin polarization and therefore of the nuclear field in a quantitative way and agrees with the experimental data, within the experimental uncertainties. This model starts with the generation of electron spins by the optical pumping process. The relevant rate of electron spin density production is proportional to the laser power  $P_L$  and decreases with increasing optical detuning  $\Delta\lambda$ . The spin polarization is then transferred from the electron spins to the nuclear spins, and we also determined the rate constant for this process. The experimental data show some

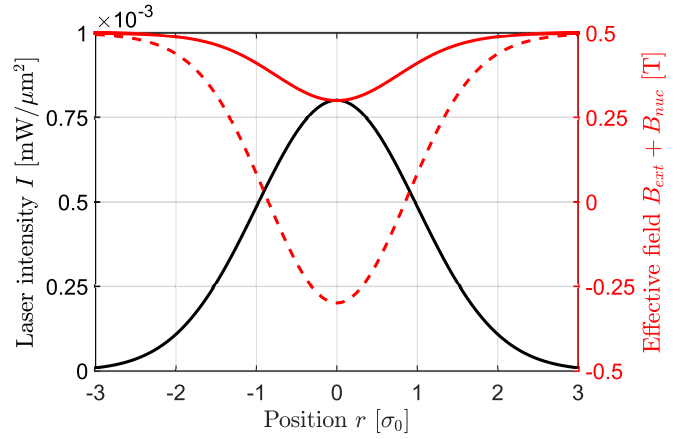


FIG. 13. Laser intensity and effective field  $B_{ext} + B_{nuc}$  with  $B_{ext} = 0.5$  T as a function of the position in the laser beam in units of  $\sigma_0 = 88 \mu\text{m}$ . The solid red line is calculated for a pumping time,  $T_{pump} = 36$  s and the dashed red line for  $T_{pump} = 271$  s.

significant deviations from the simple model, which could be explained quantitatively by taking into account that the laser beam does not illuminate the sample homogeneously, but with a roughly Gaussian profile. These results can be used to prepare the nuclear spin system e.g. for optically detected nuclear magnetic resonance experiments.

## ACKNOWLEDGMENTS

We gratefully acknowledge the support by the International Collaborative Research Centre TRR 160 “Coherent manipulation of interacting spin excitations in tailored semiconductors,” funded by the Deutsche Forschungsgemeinschaft.

- 
- [1] S. Pfalz, R. Winkler, T. Nowitzki, D. Reuter, A. D. Wieck, D. Hägele, and M. Oestreich, *Phys. Rev. B* **71**, 165305 (2005).
- [2] M. Dyakonov and V. Perel, in *Optical Orientation*, edited by F. Meier and B. Zakharchenya (Elsevier, 1984), vol. 8 of *Modern Problems in Condensed Matter Sciences*, pp. 11 – 71.
- [3] A. Ekimov and V. Safarov, *Soviet Journal of Experimental and Theoretical Physics* **12**, 1 (1970).
- [4] R. R. Parsons, *Phys. Rev. Lett.* **23**, 1152 (1969).
- [5] R. I. Dzhiyev, B. P. Zakharchenya, V. L. Korenev, P. E. Pak, D. A. Vinokurov, O. V. Kovalenkov, and I. S. Tarasov, *Physics of the Solid State* **40**, 1587 (1998).
- [6] S. E. Barrett, R. Tycko, L. N. Pfeiffer, and K. W. West, *Phys. Rev. Lett.* **72**, 1368 (1994).
- [7] T. Pietraß, A. Bifone, T. Rõõm, and E. L. Hahn, *Phys. Rev. B* **53**, 4428 (1996).
- [8] A. I. Ekimov and V. I. Safarov, *Soviet Journal of Experimental and Theoretical Physics Letters* **15**, 179 (1972).
- [9] O. S. Leifson and C. D. Jeffries, *Phys. Rev.* **122**, 1781 (1961).
- [10] G. Lampel, *Phys. Rev. Lett.* **20**, 491 (1968).
- [11] A. Abragam, *The Principles of Nuclear Magnetism* (Oxford University Press, 1967).
- [12] D. Paget, G. Lampel, B. Sapoval, and V. I. Safarov, *Phys. Rev. B* **15**, 5780 (1977).
- [13] G. Salis, D. D. Awschalom, Y. Ohno, and H. Ohno, *Phys. Rev. B* **64**, 195304 (2001).
- [14] M.J. Snelling, G.P. Flinn, A.S. Plaut, R.T. Harley, A.C. Tropper, R. Eccleston, and C.C. Phillips, *Physical Review B* **44**, 11345 (1991).
- [15] V. Kalevich, V. Korenev, and O. Fedorova, *Soviet Journal of Experimental and Theoretical Physics Letters* **52**, 349 (1990).
- [16] M. Dyakonov and V. Perel, *Soviet Journal of Experimental and Theoretical Physics* **38**, 177 (1974).
- [17] M. Dyakonov, V. Perel, V. Berkovits, and V. Safarov, *Soviet Journal of Experimental and Theoretical Physics* **40**, 950 (1975).
- [18] B. Cavenett, *Advances in Physics* **30**, 475 (1981).
- [19] M. Eickhoff, B. Lenzmann, G. Flinn, and D. Suter, *Phys. Rev. B* **65**, 125301 (2002).
- [20] M. Eickhoff, B. Lenzmann, D. Suter, S. E. Hayes, and A. D. Wieck, *Phys. Rev. B* **67**, 085308 (2003).
- [21] M. Eickhoff and D. Suter, *J. Magn. Reson.* **166**, 69 (2004).
- [22] M. Eickhoff, S. Fustmann, and D. Suter, *Phys. Rev. B* **71**, 195332 (2005).
- [23] C. Weisbuch and C. Hermann, *Phys. Rev. B* **15**, 816 (1977).
- [24] R. Hannak, M. Oestreich, A. Heberle, W. Rühle, and K. Köhler, *Solid State Communications* **93**, 313 (1995).
- [25] M. J. Snelling, E. Blackwood, C. J. McDonagh, R. T. Harley, and C. T. B. Foxon, *Phys. Rev. B* **45**, 3922 (1992).
- [26] J. Shi-Rong, X. Zhong-ying, L. Jin-sheng, L. Chang-ping, X. Ji-zong, and Z. Bao-zhen, *Acta Physica Sinica (Overseas Edition)* **3**, 384 (1994).
- [27] S. Eshlaghi, W. Worthoff, A. D. Wieck, and D. Suter, *Phys. Rev. B* **77**, 245317 (2008).
- [28] W. Hanle, *Zeitschrift fuer Physik* **30**, 93 (1924).
- [29] A. Berg, M. Dobers, R. R. Gerhardtts, and K. v. Klitzing, *Phys. Rev. Lett.* **64**, 2563 (1990).